Investigating the Impact of Ageing and Thermal Management of a Fuel Cell System on Energy Management Strategies

M. Kandidayeni [a,b] *, A. Macias [a,b], L. Boulon [a, b], S. Kelouwani [c]

[a] Hydrogen Research Institute, Department of Electrical Engineering and Computer Science, Université du Québec à Trois-Rivières, Trois-Rivières, Québec, G9A 5H7, Canada

[b] Canada Research Chair in Energy Sources for the Vehicles of the Future

[c] Hydrogen Research Institute, Department of Mechanical Engineering, Université du Québec à Trois-Rivières, Trois-Rivières, Québec, G9A 5H7, Canada

* Corresponding author.

E-mail address: mohsen.kandi.dayeni@uqtr.ca (M. Kandidayeni).

Abstract

This paper studies the impact of two significant aspects, namely fuel cell (FC) degradation and thermal management, over the performance of an optimal and a rule-based energy management strategy (EMS) in a fuel cell hybrid electric vehicle (FCHEV). To do so, firstly, a vehicle model is developed in simulation environment for a low-speed FCHEV composed of a FC stack and a battery pack. Subsequently, deterministic dynamic programming (DP), as an optimal strategy, and bounded load following strategy (BLFS), as a common rule-based strategy, are utilized to minimize the hydrogen consumption while respecting the operating constraints of the power sources. The performance of the EMSs is assessed in different scenarios. The first objective is to clarify the effect of FC stack degradation on the performance of the vehicle. In this regard, each EMS determines the required current from the FC stack for two FCs with different levels of degradation. The second objective is to evaluate the thermal management contribution in improving the performance for the new FC compared to the considered cases in scenario one. In this respect, each strategy deals with determining two control variables (FC current and cooling fan duty cycle). The results of this study indicate that negligence of adapting to the PEMFC health state, as the PEMFC gets aged, can increase the hydrogen consumption up to 24.8% in DP and 12.1% in BLFS. Moreover, the integration of temperature dimension into the EMS can diminish the hydrogen consumption by 4.1% and 5.3% in DP and BLFS respectively.

Keywords: Two-control-variable energy management strategy, dynamic programming, fuel cell hybrid electric vehicle, thermal management.

1. Introduction

1.1. Motivation and challenges

The buildup of carbon dioxide (CO2) and other greenhouse gases is causing a rise in the average temperature of the climate system, known as global warming [1]. Transportation sector is counted as one of the major contributors to the anthropogenic emission of these gases [2]. Electrification of vehicles through the introduction of hybrid electric and pure electric vehicle technologies has been considered as a potential solution for decarbonization of the conventional vehicles [3]. However, the limitations of these technologies, such as fossil fuel dependency in the former and limited driving autonomy as well as slow recharging rate in the latter, have paved the way for the emergence of other sources such as proton exchange membrane (PEM) fuel cells (FCs) in electrified vehicles [4]. Fuel cell hybrid electric vehicles (FCHEVs), which are still at an initial phase of marketing progress, typically utilize a PEMFC stack as the primary source of power and a battery pack and/or a supercapacitor (SC) as the secondary one [5, 6]. Therefore, the performance of a FCHEV is affected by many interconnected factors due to different nature of powertrain components. An appropriate energy management between power sources can enhance fuel economy and lifetime of the system. The available energy management strategies (EMSs) for FCHEVs can be classified into three types of rule-based, optimization-based, and intelligent-based [7]. Rule-based EMSs are typically designed based on heuristic techniques which are not guaranteed to be optimal or perfect, but instead adequate for attaining an immediate purpose [8]. Optimization-based EMSs theoretically offer near-optimal solutions and are also capable of drawing up new guidelines for revising the set of rules and inferential knowledge of the rule-based methods [9]. Optimization-based EMSs fall into two groups of global, optimizing the cost function over a fixed driving cycle, and real-time strategies, defining an instantaneous cost function based on the variables of the system. The former is not suitable for real-time purposes owing to the necessity to know the driving cycle in advance, but nevertheless is highly helpful for defining the optimal policy. Depending on the purpose of the project, dynamic programming (DP) (as an optimal theory-based strategy) [10, 11] and metaheuristic algorithms, such as genetic algorithm (GA) [12], (as near optimal strategies) have been abundantly used for the development of off-line global EMSs. Real-time strategies have been also formulated by using optimal theory-based methods, such as quadratic programming (QP) [13], Pontryagin's minimum principle (PMP) [14], and equivalent consumption minimization strategy (ECMS) [15] with respect to the formulation of the cost function. Intelligent-based strategies normally use the car navigation data and the history of motion for recognizing and predicting the driving condition [16]. They can be incorporated into both of ruled-based and optimization-based strategies to compensate for sensitivities and problems related to the driving condition prediction. Several EMSs based on the discussed categories and their combinations are available in the literature for hybrid vehicles. A brief summary of very recent developed strategies is given in the following paragraph to clearly highlight the contribution of this manuscript.

1.2. Literature survey

A multi-mode fuzzy EMS is proposed in [17] to minimize the hydrogen consumption in a FCHEV where a neural network-based driving condition recognition tool is utilized to select the most suitable mode of the controller. This strategy has reduced hydrogen consumption by 8.89%, compared to a normal fuzzy EMS. In [18], an EMS is proposed using the game theory, which takes into account the controller and the future driving condition to improve the operational performance. The prediction of driving condition is performed by employing Markov chain method. The results of this paper indicate that it can reduce hydrogen consumption by more than 6.82% compared to other real-time strategies. In [19], an EMS based on optimal control is proposed where the offline PMP is utilized to show the convexity of the PEMFC consumption curve and derive a formula to determine the co-state. The obtained results show that the proposed EMS shows a similar performance to the offline strategy with only 0.03% more consumption. In [20], an EMS based on load following control is proposed and shown that it benefits from simple implementation and can keep the battery operating in charge-sustained mode. In [21], a rule-based load following strategy is developed for a FC-battery vehicle where the PEMFC model is updated by a recursive algorithm to embrace the drifts owing to degradation. This EMS has been further improved in [22] and called bounded load following strategy (BLFS). The operating power of the stack is limited between two points considering the efficiency curve of

the PEMFC. These limits are refined using an optimal trajectory determined by dynamic programming. In [23], a new configuration composed of three PEMFC stacks and a battery pack is put forward. In this work, a hysteresis EMS is designed to increase the durability of the PEMFC system by utilizing each PEMFC only at a fixed operating point. In [24], a state machine based EMS is suggested for a FC-SC-battery vehicular system to extend the lifetime of the power sources by using them in their desired operational range. Moreover, the output net power of the PEMFC is maximized by regulating the oxygen excess ratio through a PID controller. In [25], a quadratic energy consumption curve of the PEMFC stack is employed in a multi-state ECMS to formulate the power management in a tram. The strategy has led to 2.5% energy consumption reduction compared to a rule-based power following strategy. In [26], an EMS is developed by using adaptive control theory and fuzzy logic control (FLC). The authors recommend updating the values for defining the FLC rules owing to the PEMFC voltage declines due to degradation after a while and under this condition the rule-based values should be reconsidered. In [27], a self-organizing map is developed as the driving condition recognizer tool to select the most suitable mode of a multi-mode FLC and an online PEMFC model is used to estimate the maximum power and efficiency points of the stack which change over time. The output of the FLC is constantly adapted to the real PEMFC state of health (SOH) and the results show an eight-percent improvement in fuel economy compared to a similar strategy without an online model. In [28], a novel degradation model of PEMFC stack is proposed to be combined in the EMS design of a FCHEV. This model is based on wavelet analysis, extreme learning machine, and genetic algorithm and considers the influence of PEMFC load current, relative humidity, temperature, and hydrogen pressure. In [29], an EMS is formulated based on model predictive control and a cost function is proposed inclusive of hydrogen, PEMFC degradation, and battery degradation costs. In [30, 31], two degradation models are proposed for PEMFC and battery and incorporated in the sizing problem of a FCHEV. In [32], an online adaptive ECMS is proposed for a FCHEV powered by PEMFC, battery, and SC. The SOH of PEMFC and battery are traced online by an adaptive filter and the results show that without SOH estimation, the charge sustenance objective of battery cannot be achieved when the power sources go under degradation. A review of health-conscious EMSs for FCHEVs is presented in [33] and it has been concluded that accurate degradation estimation should be integrated into the existing EMSs to enhance the durability of the system.

1.3. Contribution

In the light of the discussed papers, it is clear that the vast majority of the existing studies do not take the degradation of the power sources into account while designing an EMS for a FCHEV. However, recently, some studies have attempted to take this point into account [29-32]. Moreover, the developed EMSs are mainly based on one control variable as they just determine the reference current from the PEMFC stack. However, PEMFC is a multiphysics system and there is an interdependence between its power delivery and operating conditions. Fig. 1 presents the relation of power delivery with operating current and stack temperature in a 500-W PEMFC with two different levels of ageing. As it is observed, stack current and temperature have influence over the drawn power from the stack and their range varies for each power level. Moreover, the location of maximum reachable power noticeably changes as the PEMFC gets degraded. In this respect, the contributions of this work lie into the consideration of two substantial aspects. The first one is inspecting the influence of PEMFC degradation over the performance of an optimal and a rule-based EMS. This is worthwhile since it clarifies the degradation impact of PEMFC, which is a new and expensive technology, over the operation of the vehicle without combining it with the ageing effect of battery pack. The second contribution of this work is the incorporation of PEMFC thermal management into the EMS design. This is vital to be considered as PEMFC is a system and its performance is influenced not only by current but also by temperature and even other operating parameters.

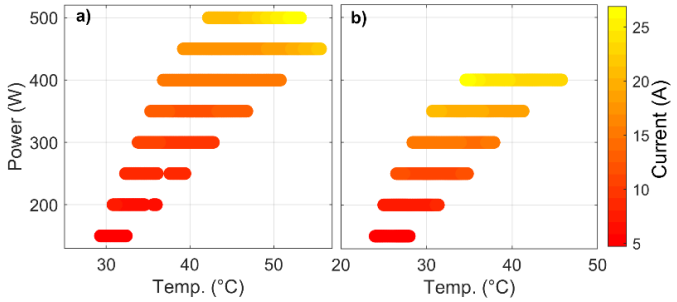

Fig. 1. The experimental characteristics of a PEMFC stack with two different degradation levels, a) new PEMFC, and b) aged PEMFC.

1.4. Methodology and paper structure

This paper proposes the formulation of two EMSs with two control variables based on DP and BLFS for a FCHEV. The control variables are PEMFC current and stack temperature, which have a crucial role in the performance of the stack. The results of the proposed strategies with two control variables are compared with the one-control-variable forms of DP and BLFS under two standard driving cycles. The one-control-variable forms of the strategies only consider the operating current and is similar to the existing EMSs in the literature. The formulation of each EMS is done for two cases of new and aged PEMFC stacks to represent the effect of ageing as well as adding the temperature dimension on the operation of the FCHEV.

The remainder of this paper is as follows. Section 2 describes the powertrain modeling of the studied FCHEV along with the characteristics of the employed power sources. Section 3 deals with the development of the EMSs. Section 4 discusses the utilized experimental set-up. Section 5 gives an account of the obtained results of the work, and finally the main conclusions from the performed study are drawn in section 6.

2. Powertrain system modeling

The studied FCHEV in this work is based on a low-speed vehicle called Nemo. The structure of this vehicle is shown in Fig. 2. The electric motor is driven by both of PEMFC stack and battery pack. The PEMFC stack is linked to the DC bus via a DC-DC converter while the battery pack is directly connected to the bus. Table 1 provides the principal powertrain parameters of this vehicle.

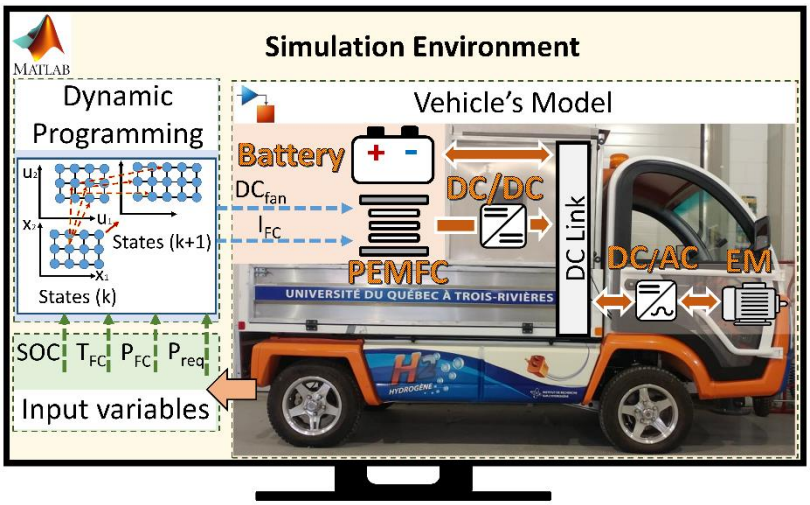

Fig. 2. The simulator for testing the EMS.

Table 1
Parameters of the vehicle

Specification	Parameter	Value
Vehicle's parameters	Rolling resistance	0.015
	Aerodynamic drag	0.42
	Frontal area (m^2)	4
	Density of air (kg/m^3)	1.2
	Mass factor	1.035
	Mass (kg)	896
	Maximum speed (km/h)	40
3-phase induction machine	Power (W)	5690
	Frequency(Hz)	131.1
FC system	Rated power (kW)	4
Battery	voltage (V)	73
	Capacity (Ah)	6

A vehicle's movement alongside its moving direction is entirely defined by the forces acting on it in that direction. Fig. 3 demonstrates the forces acting on a vehicle going up a slope [34, 35].

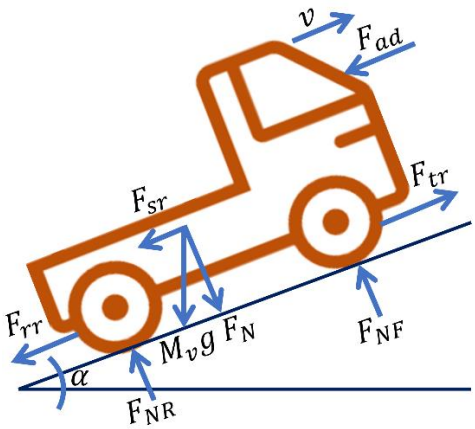

Fig. 3. Vehicle's dynamics while moving uphill

According to Newton's second law, vehicle acceleration can be written as:

$$\frac{dv(t)}{dt} = \frac{\sum F_{tr} - \sum F_r}{\delta M_v} \tag{1}$$

Where v is the speed of the vehicle, $\sum F_{tr}$ is the total tractive effort of the vehicle, $\sum F_r$ is the total resistance, M_v is the total mass of the vehicle, and δ is the mass factor that equivalently converts the rotational inertias of rotating components into translational mass. According to Fig. 3, in the longitudinal direction, the major external forces acting on the vehicle includes tire rolling resistance (F_{rr}), aerodynamic drag (F_{ad}), slope resistance (F_{sr}), and the tractive effort of the vehicle (F_{tr}). The dynamic equation of vehicle motion along the longitudinal direction is expressed by [23, 24, 32, 36]:

$$\begin{cases} \delta\, M_v \frac{dv}{dt} = F_{tr} - (F_{rr} + F_{ad} + F_{sr}) \\ F_{sr} = M_v\, g\, sin\left(\frac{\alpha\pi}{180^\circ}\right) \\ F_{rr} = -C_f\, M_v\, g\, cos\left(\frac{\alpha\pi}{180^\circ}\right) \\ F_{ad} = 0.5\, \rho_a\, C_d\, A_f\, v^2(t) \end{cases} \tag{2}$$

where g is the gravitational acceleration (m/s^2), α is the road angle in degrees, C_f is the rolling friction coefficient, ρ_a is the air density (kg/m^3), C_d is the aerodynamic drag coefficient, A_f is the vehicle frontal area (m^2), and $v(t)$ is the vehicle velocity (m/s).

The requested power in the bus (P_{Bus}) by the drive of the induction machine is calculated by:

$$\begin{cases} P_{Bus} = \frac{P_{wheel}}{\eta_{EM}\,\eta_t\,\eta_{DC-AC}} \\ P_{wheel} = F_{tr} \times v(t) \end{cases} \quad (3)$$

where P_{wheel} is the required power at wheels, η_t is the transmission efficiency (92%), η_{EM} is the motor average efficiency (90%), and η_{DC-AC} is the inverter efficiency (95%). As shown in Fig. 2, the PEMFC stack and battery pack are connected to the DC bus. Therefore, the relationship of PEMFC power (P_{FC}), battery power (P_{Bat}), and the requested power in the bus can be expressed as:

$$P_{Bus} = P_{FC}\eta_{DC-DC} + P_{Bat} \quad (4)$$

2.1. PEMFC modeling

The utilized model in this paper takes the temperature, current, and pressure as inputs and estimates the voltage of the stack. It is based on a semi-empirical equation, suggested by Mann et al [37], which calculates the stack voltage for a number of cells connected in series.

$$V_{FC} = N(E_{Nernst} + V_{act} + V_{ohmic} + V_{con}) \quad (5)$$

$$E_{Nernst} = 1.229 - 0.85 \times 10^{-3}(T - 298.15) + 4.3085 \times 10^{-5}T[\ln(P_{H2}) + 0.5\ln(P_{O2})] \quad (6)$$

$$\begin{cases} V_{act} = \xi_1 + \xi_2 T + \xi_3 T ln(CO_2) + \xi_4 T ln(i_{FC}) \\ CO_2 = \frac{P_{O2}}{5.08\times10^{-6}\exp(-498/T)} \end{cases} \quad (7)$$

$$V_{ohmic} = -i_{FC}R_{internal} = -i_{FC}(\zeta_1 + \zeta_2 T + \zeta_3 i_{FC}) \quad (8)$$

$$V_{con} = Bln(1 - \frac{i_{FC}}{i_{FC,max}}) \quad (9)$$

Where V_{FC} is the output voltage (V), N is the number of cells, E_{Nernst} is the reversible cell potential (V), V_{act} is the activation loss (V), V_{ohmic} is the ohmic loss (V), V_{con} is the concentration loss (V), T is the stack temperature (K), P_{H2} is the hydrogen partial pressure in anode side (N m^{-2}), P_{O2} is the oxygen partial pressure in cathode side (N m^{-2}), $\xi_n (n = 1 \dots 4)$ are the semi-empirical coefficients based on fluid mechanics, thermodynamics, and electrochemistry, CO_2 is the oxygen concentration (mol cm^{-3}), i_{FC} is the PEMFC operating current (A), $R_{internal}$ is the internal resistor (Ω), $\zeta_n (n = 1 \dots 3)$ are the parametric coefficients, B is a parametric coefficient (V), i_{FC} is the actual current (A), and $i_{FC,max}$ is the maximum. The semi-empirical parameters of the voltage model have been tuned by a metaheuristic optimization algorithm. The explanation of the optimization algorithm employment for extracting the parameters is considered redundant herein as it has been comprehensively discussed in [38]. The obtained values for the parameters are: ξ_1=-0.995, ξ_2=2.1228×10^{-3}, ξ_3=2.1264×10^{-5}, ξ_4=-1.1337×10^{-4}, ζ_1=-0.024, ζ_2=7.60×10^{-5}, ζ_3=-1.06×10^{-3}, B=0.4970. The power of the PEMFC system (P_{FCS}) is achieved by deducting the PEMFC stack power (P_{FC}) from the consumed power by the cooling fan (P_{fan}) and hydrogen valve (P_{Valve}). The consumed power by the purge valve is ignored in this paper since it has a fixed cyclic purging (every 10 s for duration of 100 ms).

$$P_{FCS} = P_{FC} - P_{fan} - P_{Valve} \quad (10)$$

$$P_{FC} = V_{FC} \times I_{FC} \quad (11)$$

$$P_{fan} = c_1 {D_{fan}}^2 + c_2 D_{fan} + c_3 \quad (12)$$

$$P_{Valve} = V_{Valve} \times I_{Valve} \quad (13)$$

Where the empirical parameters (c_1 = 0.001365, c_2 = 0.1139, and c_3 = -0.9946) are determined by experiments, as explained in section 4, D_{fan} is the cooling fan duty cycle, V_{Valve} is the voltage of the hydrogen valve, and I_{Valve} is the current of the hydrogen valve. The consumed power of the hydrogen valve is constant as it is normally open while the PEMFC operates.

The stack temperature is calculated based on the energy conservation law [39, 40], where the forced convection equation includes the effect of the blower in the model.

$$m_{st} C_{st}\, dT_{st}/dt = P_{loss} - Q_{Nat} - Q_{Forced} \tag{14}$$

Where m_{st} is the stack mass (4.2 kg), C_{st} is the specific heat capacity of stack (J/kg K) [40], T_{st} is the stack temperature (K), P_{loss} is the heat loss in form of entropy in the system, Q_{Nat} is the natural convection, and Q_{Forced} is the forced convection. The change of Gibbs free energy in a system is defined in terms of the change of enthalpy (ΔH_f), temperature (T) and entropy change (ΔS_f):

$$\Delta G_f = \Delta H_f - T\Delta S_f \tag{15}$$

As discussed in [41, 42], presuming that the PEMFC is an isolated system, the change of entropy can be considered as zero and the Gibbs free energy will be equal to the enthalpy variation (ΔH_f). Under this condition, the maximum voltage (V_{max}) generated by the overall conversion of enthalpy into electrical energy is calculated by:

$$V_{max} = -\frac{\Delta H_f}{n_e F} \tag{16}$$

where F is the Faraday constant (96485 $C\ mol^{-1}$), n_e is the number of electrons which is two in case of hydrogen in the overall PEMFC reaction ($H_2 + \frac{1}{2}O_2 \rightarrow H_2O$), $\Delta H_f = -285.84$ kj mol^{-1} if the water product is in liquid form, and $\Delta H_f = -241.83$ kj mol^{-1} if the water product is in vapor form. The higher value for ΔH_f is used in this work. It is known as the higher heating value (HHV), which is in fact the energy content of hydrogen.

Under the condition $I_{FC}(t) > 0$, the delivered voltage by the cell is lower than the standard potential. Therefore, it is impossible to reach V_{max} in a PEMFC as there is always heat loss in form of entropy in the system. This heat loss is given by:

$$P_{loss} = I_{FC}(NV_{max} - V_{FC}) \tag{17}$$

The natural convection is calculated by:

$$Q_{Nat} = h_{Nat}\, A_{Nat}(T_{st} - T_{ca}) \tag{18}$$

where h_{Nat} is the natural heat transfer coefficient (14 W/m^{2}K) [39], A_{Nat} is the total surface area of the 500-W Horizon PEMFC (0.1426 m^2) which has been obtained from the available dimensions in the manual of the device, and T_{ca} is the ambient temperature (K). The forced convection which is the heat rate removed from rectangular channels of the PEMFC by the two blowers is obtained by:

$$Q_{Forced} = V_{air}\, \rho_{air}\, A_{ch}\, C_p(T_{st} - T_{ca}) \tag{19}$$

where V_{air} is the air velocity (m/s), ρ_{air} is the ambient air density (1.267 kg/m^3), A_{Ch} is the effective cross-sectional area of the channel, and C_p is the air specific heat capacity (1005 J/kg K). The effective area of the channel is determined by:

$$A_{ch} = \delta\, A_{inlet} \tag{20}$$

where A_{inlet} is the total cross-sectional area perpendicular to the air flow running through the stack by the blowers (0.22m×0.13m) and δ is a correction factor for obtaining the effective area. The air velocity is computed by:

$$V_{air} = a_1 D_{Fan} + a_2 \quad (21)$$

where a_1 and a_2 are empirical parameters determined by experiments, as described in section 4. Hydrogen flow ($H_{2,flow}$) is calculated by an empirical equation [43] as:

$$H_{2,flow} = a\, i_{FC} + b\, D_{fan} + c \quad (22)$$

where the fitting parameters (a = 0.1539, b = -0.05308, c = 1.657) are attained by experimental data and the unit of hydrogen flow is SLPM.

2.2. Battery modeling

A lithium-ion battery pack is employed to assist the PEMFC stack to deliver the requested power from the electric motor side. The specifications of the battery are listed in Table 2. An internal resistance based model is used for modeling the behavior of this battery [44]. Fig. 4 shows the relationship of battery SOC with each of open circuit voltage (U_{bat-OC}), internal resistance changes in charge ($R_{bat-charge}$), and internal resistance changes in discharge ($R_{bat-discharge}$). The data regarding the internal resistance changes in charge and discharge come from the experimental tests performed by the National Renewable Energy Laboratory (NREL) [44, 45]. The battery current (I_{bat}), bus voltage (U_{bus}), and SOC are determined by:

$$I_{Bat} = \frac{(U_{Bat-OC} - \sqrt{U_{Bat-OC}{}^2 - 4 \times R_{Bat} \times P_{Bat}}}{2 \times R_{Bat}} \quad (23)$$

$$U_{Bus} = U_{Bat-OC} - I_{Bat} \times R_{Bat} \quad (24)$$

$$SOC(t_f) = SOC(t_0) - \eta_C \frac{\int_{t_0}^{t} I_{Bat} dt}{C_{Bat}} \quad (25)$$

where P_{Bat} is the battery pack power, C_{Bat} is the capacity, and η_C is the coulombic efficiency only during charge (0.98) [36].

Table 2
The specifications of the employed battery

Specification	Parameter	Value
SAFT Rechargeable lithium-ion battery cell	Maximum current continuous	C/1 A
	Capacity	6 Ah
	Nominal voltage	3.65 V
	No. of cells in series	20
	Cell mass	0.34 kg
	Coulombic efficiency	0.99

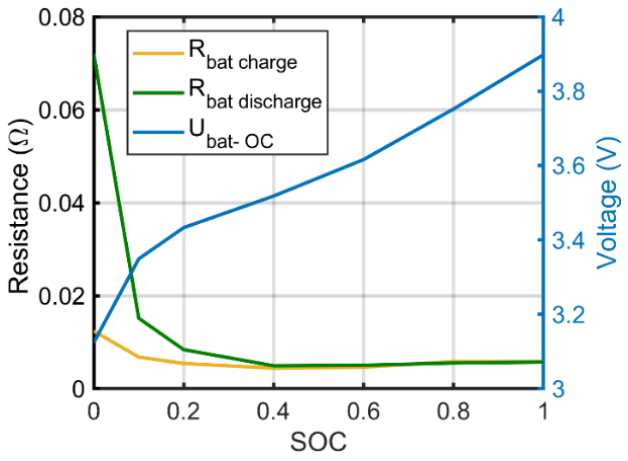

Fig. 4. The relationship of SOC with U_{bat-OC} and R_{bat} per cell.

3. Energy management strategy

In order to explore the impact of ageing and thermal management in the performance of a FCHEV, two different EMSs are developed in this paper. The first one is based on DP which is considered as an optimal strategy and requires a priori knowledge of the driving cycle. This strategy illustrates the influence of the mentioned factors in an offline case. The second one is BLFS which is a rule-based strategy and does not need an information about the driving profile. This strategy highlights the effect of the considered factors in a real-time case study. These EMSs are discussed in more details hereinafter.

3.1. Dynamic programming with two control variables

The model of a FCHEV can be expressed as a nonlinear state space model. One of the most common methods which focuses on the optimal control of nonlinear, time-variant, constrained, discrete-time approximations for continuous-time dynamic models is deterministic DP. Such DP tools have been already employed successfully in the energy management problem of different HEVs [10, 11, 46]. In this work, the MATLAB function introduced in [10] is utilized to solve the discrete-time optimal-control problem using DP algorithm. The proposed DP here minimizes the hydrogen consumption by determining the optimal trajectories of PEMFC stack current and cooling fan duty cycle. It should be noted that more complex cost functions have not been considered in this study as the main purpose is to clarify the impacts of degradation and temperature dimension consideration in the hydrogen consumption rather than reducing the degradation through time. However, this work paves the way for formulating more complex cost functions in future to reduce both hydrogen consumption and the occurrence of degradation in the PEMFC to the utmost.

The main states of the system are battery SOC and stack temperature. Moreover, the power of PEMFC system is also considered as a state to be able to prevent sudden and big changes in the drawn power from the stack. It should be noted that according to [47], a dynamic limitation of 50 Ws^{-1}, which means a maximum of 10% of the maximum power per second for rising, and also 30% of the maximum power per second for falling, as suggested in [22], have been considered for the operation of the PEMFC system. The steady space model equations can be described as:

$$\begin{cases} x_{k+1} = f(x_k, u_k, v_k, a_k, i_k) + x_k \\ x = [SOC, T_{st}, P_{FCS,SV}] \\ u = [I_{FC,CV}, D_{fan}] \end{cases} \quad (26)$$

where x_k is the state vector, u_k is the control variable vector, v_k is the vehicle velocity, a_k is the vehivle acceleration, i_k is the gear number, $P_{FCS,SV}$ is the PEMFC power as a state variable, and $I_{FC,CV}$ is the state current as a control variable. As the driving cycle is known in advance, the vehicle velocity (v_k), acceleration

(a_k) and gear number (i_k) can be included in the model function and as a result the steady space model will be simplified to:

$$x_{k+1} = f(x_k, u_k) + x_k, \quad k = 0,1, \dots N-1 \tag{27}$$

$$N = \frac{T_F}{T_s} + 1 \tag{28}$$

where T_F is the final time of the driving cycle and T_s is the sampling time. The minimization of the hydrogen consumption is formulated as:

$$J = min \sum_{k=0}^{N-1} H_2(u_k, k) \tag{29}$$

The applied constrains to the control variables are as follows:

$$\begin{cases} I_{FC,min} \le I_{FC,CV}(k) \le I_{FC,max} \\ D_{fan,min} \le D_{fan}(k) \le D_{fan,max} \end{cases} \tag{30}$$

where $I_{FC,min}$ and $I_{FC,max}$ are the minimum and maximum current of the PEMFC stack ($I_{FC,CV} \in [0, 27]$), and $D_{fan,min}$ and $D_{fan,max}$ are the minimum and maximum duty cycle of the cooling fan ($D_{fan} \in [\,34, 100]$). The constraints on the state variables are defined as:

$$\begin{cases} SOC_{min} \le SOC(k) \le SOC_{max}, & (SOC_{min} = 50\ \%, SOC_{max} = 90\ \%) \\ T_{st,min} \le T_{st}(k) \le T_{st,max}, & \left(T_{st,min} = 25\ ^\circ C, T_{st,max} = 65\ ^\circ C\right) \\ P_{FCS,SV,min} \le P_{FCS,SV}(k) \le P_{FCS,SV,max} & \left(P_{FCS,SV,min} = 0\ W,\ P_{FCS,SV,max} = 500\ W\right) \\ \Delta P_{FC,SV,min} \le \Delta P_{FC,SV}(k) \le \Delta P_{FC,SV,max} & \left(\Delta P_{FC,SV,min} = -150\ \mathrm{Ws^{-1}},\ \Delta P_{FC,SV,max} = 50\ \mathrm{Ws^{-1}}\right) \end{cases} \tag{31}$$

3.2. Bounded load following strategy

A commonly employed rule-based strategy, which is known as BLFS in the literature [21, 22], is used as the second EMS in this study. BLFS is based on a hysteresis scheme to distribute the power between the PEMFC stack and battery pack. It restricts the operation of the PEMFC stack between maximum efficiency (ME) and maximum power (MP) points and mainly has three modes of operation, namely ON/OFF, $P_{FC,min}$, and $P_{FC,max}$. These modes are used with regard to the level of battery SOC and requested power. To assure a low level of hydrogen consumption, the ME point of the PEMFC is employed as the P_{FC_min} mode. This is due to the fact that the level of hydrogen consumption and degradation is higher when operating between the open circuit voltage and PEMFC ME point. Hence, when the PEMFC is turned on, the ME mode is activated. P_{FC_max}, which sets the stack on its MP, is used when the battery SOC reaches the minimum SOC level. The only time that PEMFC works between OFF and $P_{FC,min}$ is the transitions from OFF to $P_{FC,min}$ due to the slew rate limitations. The details of BLFS are available in [22]. The constraints regarding the battery SOC and PEMFC slew rates are the same as DP strategy in the previous section. It should be noted that BLFS determines the requested power from the PEMFC, and this power is then supplied by utilizing an appropriate combination of current and temperature to reduce the hydrogen consumption in full measure. The combination of current and temperature levels is selected by using an optimal power line extracted from the PEMFC as explained in the subsequent section.

4. Experimental set-up

As the main objectives of this paper are to investigate the effect of degradation and thermal management over the performance of an EMS, the experimental data of two 500-W Horizon PEMFCs with different levels of degradation are employed to form a realistic perception of these effects. The experimental data are gathered from a developed test bench in Hydrogen Research Institute of Université du Québec à Trois-Rivières

(UQTR), as shown in Fig. 5. In this set-up, a Horizon H-500 air breathing PEMFC is connected to a National Instrument CompactRIO through its controller. The PEMFC controller carries out the following tasks:

- Controlling the stack temperature by acting on the blower.
- Opening the hydrogen valve.
- Controlling the purging interval of the purge valve.

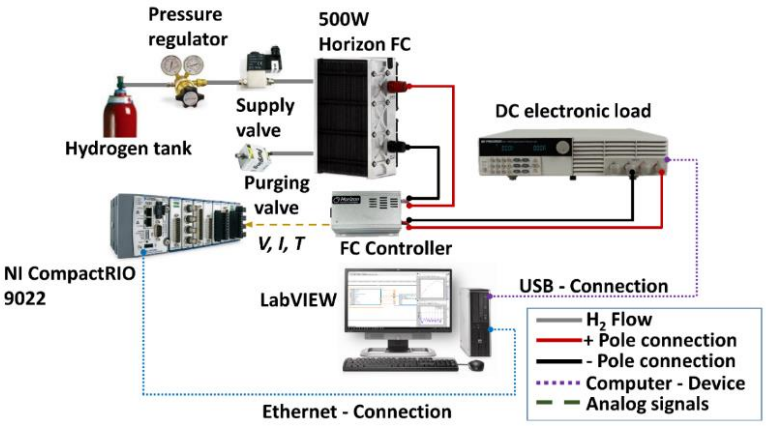

Fig. 5. The developed PEMFC test bench in Hydrogen Research Institute of UQTR

The mounted axial fan is responsible for cooling down the stack and supplying the necessary oxygen. The hydrogen supply subsystem comprises a hydrogen tank, a pressure regulator, a hydrogen supply valve, a hydrogen purging valve, and a mass flowmeter. The pressure of hydrogen is adjusted between 0.5 and 0.6 Bar. In the anode side, the hydrogen valve provides the PEMFC with dry hydrogen which can have a flow rate between 0 to 7 l/min with respect to the drawn power from the stack. The voltage of the Hydrogen valve is V_{Valve} =12 V, and the current of the Hydrogen valve is I_{Valve} = 0.72 A. Moreover, the purge valve, as the anode outlet, expels the excess water, hydrogen, and nitrogen every 10 s for a duration of 100 ms to refill the anode volume with fresh hydrogen. The pressure difference between the anode and the cathode must not exceed 0.5 bar to avoid membrane damages. The information between the CompactRIO and the PC is transferred by an Ethernet connection every 100 ms. Temperature, current, and voltage of the FC system are recorded and used for the modeling. An 8514 BK Precision DC Electronic Load is used to request load profiles from the PEMFC. Fig. 6 demonstrates the consumed power of the cooling fan by measuring the voltage and current of the fan in different duty cycles. The fitting parameters in (12) have been extracted from Fig. 6. Fig. 7 illustrates the relationship between the air speed and duty cycle of the cooling fan. The empirical parameters of (21) have been obtained from this figure.

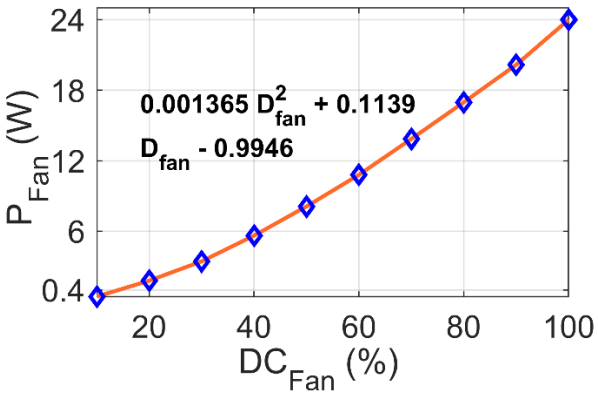

Fig. 6. The 500-W Horizon PEMFC Cooling fan power consumption respecting the duty cycle.

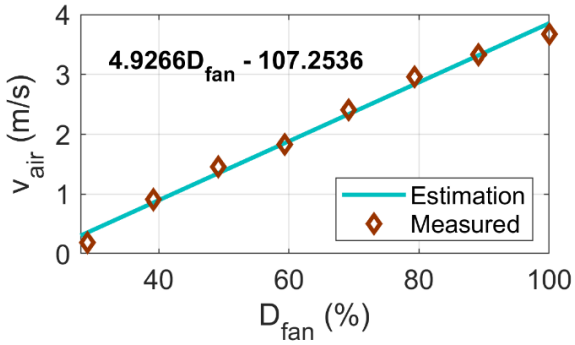

Fig. 7. Air velocity with respect to the cooling fan duty cycle

Fig. 8 presents the experimental characteristics of the aged and new PEMFCs in terms of power delivery and hydrogen consumption. Fig. 8a shows the relationship of power, temperature, and current for better appreciation of the current and temperature interdependence. From Fig. 8a, it is realized that a specific level of requested power from the PEMFC can be supplied by different combinations of current and temperature. One point which has the lowest current in each power level is selected and shown by a circle marker for the new FC and a diamond marker for the aged FC. In fact, the circle and diamond markers in Fig. 8a show the location of optimal current and its corresponded temperature for supplying each power level. Connecting all the circle markers leads to the realization of an optimal temperature-vs.-current line for the new FC and connecting all the diamond markers gives an optimal temperature-vs.-current line for the aged FC. Fig. 8b indicates the optimal line of hydrogen consumption for each of the new and aged PEMFCs. It should be noted that the presented circle and diamond markers in Fig. 8b are the corresponding points of the optimal markers shown in Fig. 8a. This confirms that each selected combination of temperature and current in Fig. 8a leads to the supply of power by the PEMFC with the lowest hydrogen consumption. From this figure, it is also observed that there is a noticeable difference between the hydrogen consumption of a new and an aged PEMFC. The specifications of this PEMFC are listed in Table 3. According to Table 1, Nemo vehicle requires a 4-kW FC system. Hence, the PEMFC output voltage in the emulator of this work is scaled up after the DC-DC converter to satisfy the requested power in the bus.

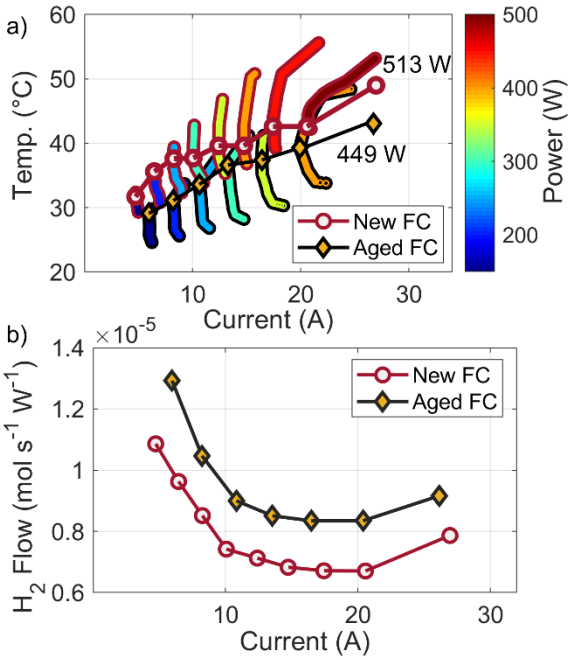

Fig. 8. The experimental characteristics of new and aged PEMFCs, a) temperature-current relationship, and b) Hydrogen flow-current relationship

Table 3
The specifications of the Horizon H-500 FC

PEMFC Technical specification	
Type of FC	PEM
Number of cells	36
Max Current (shutdown)	29 A
Hydrogen pressure	50-60 kPa (0.5-0.6 Bar)
Rated H_2 consumption	7 SLPM
Ambient temperature	5 to 30 °C
Max stack temperature	65 °C
Cooling	Air (integrated cooling fan)

5. Results and discussion

A full account of the results obtained from different sections of this paper is provided in this section. Firstly, the developed PEMFC model is validated by using some experimental data. Subsequently, the scenarios for assessing the performance of each EMS are described. Afterwards, the results of the optimal and the rule-based EMSs come under a close scrutiny in two separate sections. Finally, a synopsis of the obtained outcomes is presented.

5.1. PEMFC model validation

The performance of the PEMFC model has been examined under a random current and cooling fan duty cycle profile. Fig. 9a demonstrates the applied current to the PEMFC. Fig. 9b illustrates the cooling fan duty cycle as well as the estimation of stack temperature. Moreover, the estimation of the PEMFC voltage is presented in Fig. 9c. From Fig. 9, it is observed that the utilized model is able to satisfactorily emulate the behavior of the real PEMFC stack.

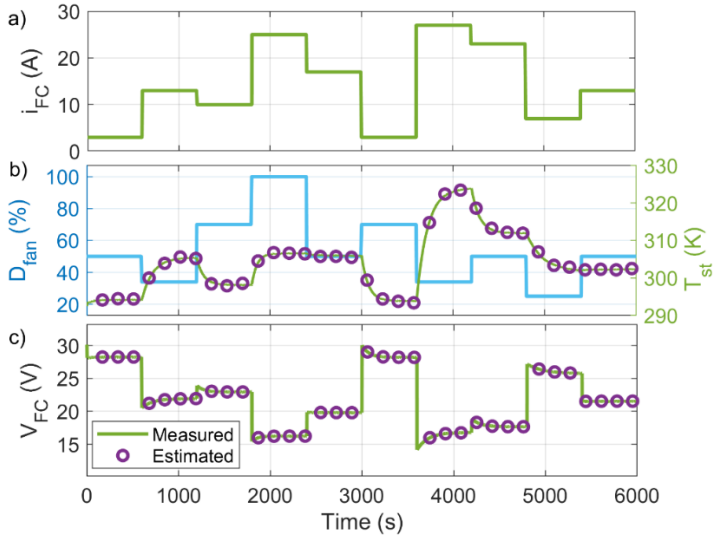

Fig. 9. Performance validation of the PEMFC model, a) applied current to the PEMFC, b) cooling fan duty cycle and the corresponding temperature estimation, and c) voltage estimation.

5.2. The considered scenarios for testing the energy management strategies

The performance of the formulated EMSs is explored under two driving cycles, namely worldwide harmonized light-duty vehicles test cycles (WLTC_class 2) and West Virginia Interstate Driving Schedule (CYC_WVUINTER). WLTC is a rather new global standard for defining the levels of pollutants and fuel consumption of traditional and hybrid cars. Fig. 9 shows the employed driving cycles and their corresponding requested power curves. According to this figure, WLTC_class 2 contains three driving regimes of low, medium, and high speed. However, CYC_WVUINTER is mainly composed of a high-speed driving regime.

This driving profile helps to better appreciate the effect of temperature inclusion as it has less start-stop cycles.

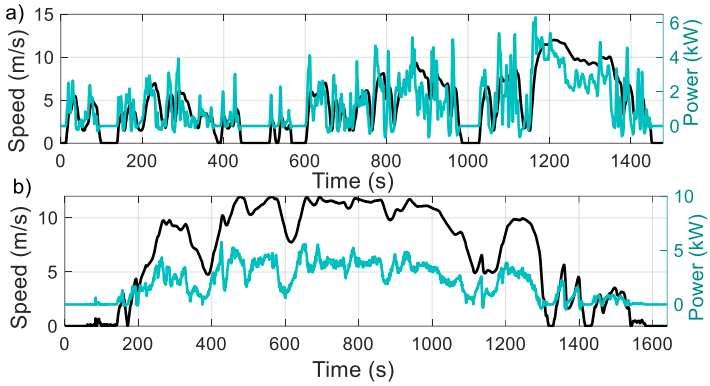

Fig. 9. The utilized driving cycles and the obtained requested power for DP formulation, a) WLTC_class 2, and b) CYC_WVUINTER.

Each of the EMSs is examined by considering four cases studies:

- EMS for tuning one control variable for the new PEMFC (1D – New FC): In this case study, the required current from the new PEMFC is determined by each EMS while the PEMFC stack temperature is regulated by using the same policy as the original PEMFC fan controller. In this regard, the cooling fan duty factor is kept constant around 34% and only if the temperature reaches 60 ℃, the duty cycle switches to 100% to avoid reaching the limiting stack temperature, which is 65 ℃. This policy for controlling the cooling fan duty cycle has been adopted based on the observation of the 500-W Horizon PEMFC operation with its controller.
- EMS for tuning one control variable for the aged PEMFC (1D – Aged FC): In this case study, the required current from the aged PEMFC is determined by each EMS while the PEMFC stack temperature is regulated by using the original PEMFC fan controller policy.
- EMS for false-input case study (1D – FI) with one control variable: The false-input case study has been adopted in a specific way for each of DP and BLFS strategies. Regarding the DP strategy, the obtained optimal control policy from 1D – New FC case is employed while the used PEMFC is the aged one. This case study shows the effect of PEMFC degradation on the performance of the optimal EMS. Concerning the BLFS, the aged PEMFC is employed while the operating constraints, such as ME and MP points, are set according to the new PEMFC. This case study clarifies the influence of not updating the PEMFC characteristics over the fuel economy of the vehicle.
- EMS for tuning two control variables for the new PEMFC (2D – New FC): The second scenario investigates the performance of each strategy with two control variables for the new PEMFC. In fact, each strategy determines the current and duty cycle of the cooling, which regulates the temperature. The results of this case study are comparable with 1D – New FC case and illustrate the influence of temperature dimension inclusion over the performance of the vehicle. The formulation of EMSs with two control variables has not been repeated for the aged PEMFC and false input cases to avoid the discussion of similar analyses in the paper.

5.3. Dynamic programming results

Fig. 10 illustrates the obtained results from running DP strategy for WLTC_class 2 driving cycle in the four above-explained case studies. Fig. 10a presents the scaled-up drawn power signals from the PEMFC for each case study. According to this figure, DP has adopted a specific policy for each of 1D – New FC and 1D – Aged FC case studies, which implies that the optimal policies of power sharing cannot be the same for the aged and the new PEMFC. Fig. 10b, Fig. 10c, and Fig. 10d present the battery SOC level, the real-scale drawn current from PEMFC, and stack temperature evolution respectively.

Comparison of 1D – New FC and 1D – Aged FC case studies shows that from 0 to almost 600 s, the SOC descends to around 50% for both strategies. However, from 600 s to almost 1000 s, the strategies show completely different behavior. On the one hand, the 1D – New FC increases the drawn current to a high of 22 A. Then, it drops to almost 17 A for almost 300 s and gradually decreases to 0. This variation causes fluctuation in the stack temperature (from 27 ℃ to almost 40 ℃) and battery SOC (from a high of 50% to a low of 80%). The 1D – Aged FC, on the other hand, sustains the battery SOC level around 55% by gradually increasing the current and temperature within this interval. From 1000 s to the end, the 1D – Aged FC increases the current to almost 20 A which causes a surge in the stack temperature while the 1D – New FC tries to use less current by discharging the battery and cooling down the stack.

Regarding the 1D – FI case study, it demands the same power signal from the PEMFC as 1D – New FC since it uses the same DP policy. However, the PEMFCs' health states are different. Fig. 10b also shows that 1D – FI and 1D – New FC have the same battery SOC variations since they extract the same power from the aged and new PEMFCs respectively. Nonetheless, Fig. 10c illustrates that in 1D – FI case study, the aged PEMFC needs to operate in higher current levels, especially between 700 s to 1000 s, to supply the same power as the new PEMFC. The stack temperature is also higher in this period for the 1D – FI case.

The comparison of 1D – New FC and 2D – New FC DPs indicates that the DP with two control variables has ended up with more variations compared to the one with one control variable. It stems from the fact that in 2D – New FC, each specific level of power can be supplied by different combinations of current and fan duty cycle (which leads to different temperature levels). Therefore, the 2D – New FC DP attempts to choose the combination that leads to the lowest hydrogen consumption. However, there are not many combinations of current and fan duty cycle for the case of 1D – New FC DP.

Looking more closely at the performance of the 2D – New FC, it is seen that from 0 to almost 600 s, the requested current from the stack is higher than the 1D – New FC. This results in warming up the stack to a desired level during this interval (35 ℃ to 40 ℃) and sustaining the battery SOC level around 60%. From 600 s to almost 1000 s, the 2D – New FC strategy virtually keeps the stack temperature between 35 ℃ to 40 ℃ and SOC level between 60% to 65%. From 1000 s to the end, this strategy shows a smooth fluctuation to finish in the same SOC level as initial.

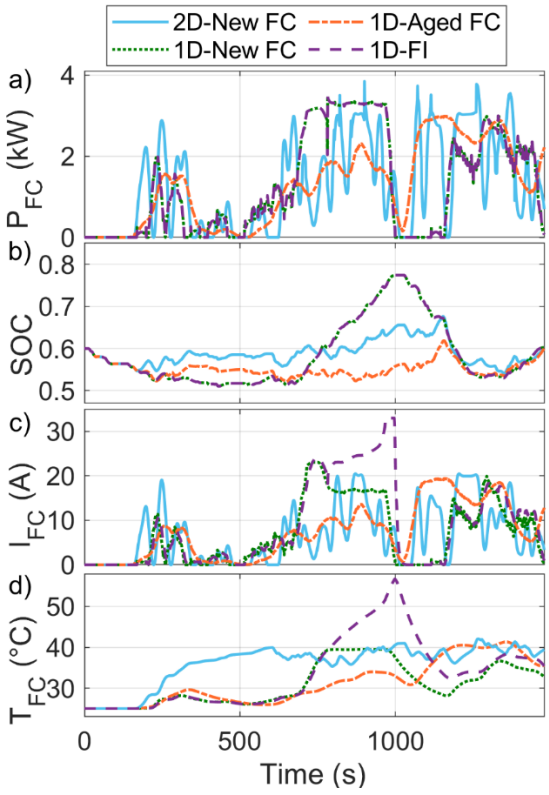

Fig. 10. DP results for WLTC_class 2 driving cycle, a) the drawn power from PEMFC stack (scaled-up signal), b) battery SOC, c) the real scale drawn current from the stacks, and d) the real scale stack temperature evolution.

Fig. 11 represents the results of DP strategy for the CYC_WVUINTER driving cycle. Fig. 11a presents the scaled-up power provided by the PEMFC in each scenario and the corresponded battery SOC, stack current, and temperature are shown in Fig. 11b to Fig. 11d respectively.

Comparing the 1D – New FC and 1D – Aged FC cases, it is seen that the DP for the new FC discharges the battery up to 300 s and after that it turns on the PEMFC to recharge the battery and meet the requested power. However, the DP for the aged FC decides to charge the battery to a high of 75% in this interval. From 300 s to almost 1100 s, both strategies increase the drawn current from the PEMFC with slightly different fluctuations to meet the requested power and in both cases the stack temperature rises. From 1100 s to the end, the stack temperature in both cases decreases, and finally, they finish in the same SOC level.

With regard to 1D – FI case study, it can be observed that the aged PEMFC requires to work in higher current and temperature levels from almost 400 s to 1400s to supply the requested power and sustain the same battery SOC level as 1D – New FC.

Concerning the 2D – New FC, it is observed that this strategy sustains the SOC level around 60% up to 300 s. From 300 s to almost 1100 s, it increases the drawn current from the PEMFC with some oscillations to meet the requested power which in turn increases the stack temperature. From 1100 s to the end, the strategy tries to keep the desired temperature level.

Fig. 12 compares the PEMFC current distribution of 1D – New FC and 2D – New FC DPs for both driving cycles. From Fig. 12a, it is seen that both strategies work in various levels as the WLTC_class 2 driving cycle contains several stops and low-speed traffic conditions. However, in case of CYC_WVUINTER driving cycle, the strategies, specifically the one with two control variables, can operate more time in the efficient current zone which is between 17 A to 21 A, according to the presented characteristics in Fig. 8.

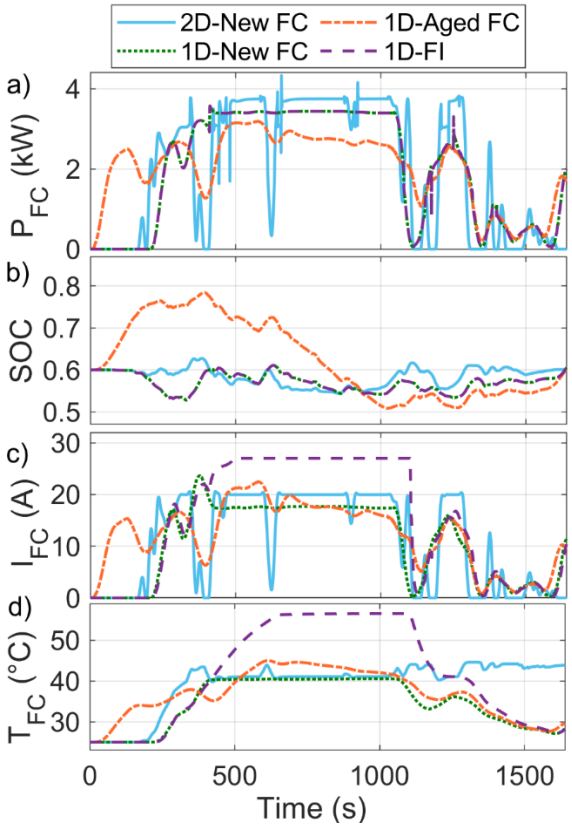

Fig. 11. DP results for CYC_WVUINTER driving cycle, a) the drawn power from PEMFC stack (scaled-up signal), b) battery SOC, c) the real scale drawn current from the stacks, and d) the real scale stack temperature evolution.

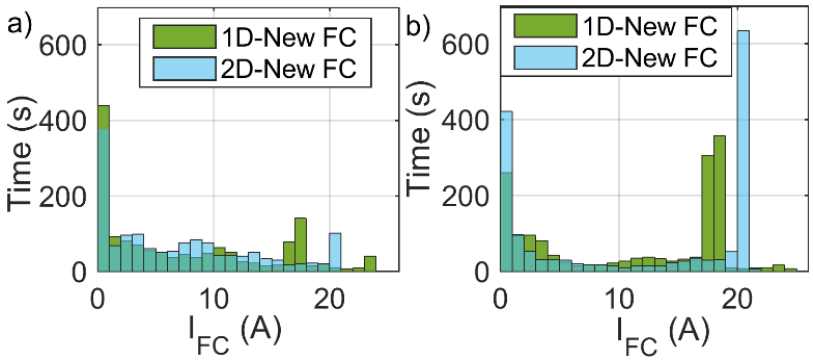

Fig. 12. PEMFC current distribution of 1D – New FC and 2D – New FC DPs for: a) WLTC_class 2, and b) CYC_WVUINTER.

Fig. 13 compares the consumed hydrogen, which is the most important factor in this work, for all the previously-discussed cases in DP strategy. According to this figure, the hydrogen economy decreases as the PEMFC gets aged. By comparing the 1D – New FC and 1D – Aged FC cases, it can be seen that hydrogen consumption increases by 14.7% in WLTC_class 2 and 11.7% in CYC_WVUINTER. Moreover, it is observed if the PEMFC gets aged and the DP policy remains the same (1D – FI case study), the hydrogen consumption increases by 24.8% compared to 1D – New FC case and 8.7% compared to 1D – Aged FC in WLTC_class 2. In CYC_WVUINTER, 1D – FI case study escalates the hydrogen consumption by 20.2% and 7.6% compared to 1D – New FC and 1D – Aged FC respectively. The obtained results from 1D – FI case study shows that the energy management policy should be adapted to the real health state of the PEMFC stack, otherwise it leads to poor performance of the strategy. Regarding the influence of thermal management incorporation into the EMS formulation, comparison of 1D – New FC and 2D – New FC DPs shows that the hydrogen consumption is declined by 2.91% and 4.1% in WLTC_class 2 and CYC_WVUINTER respectively.

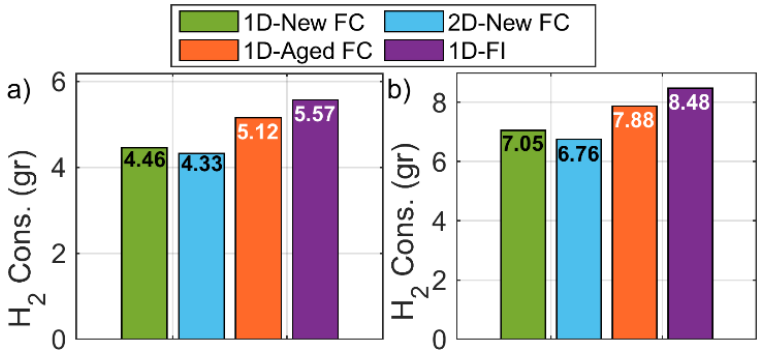

Fig. 13. Hydrogen consumption a) WLTC_class 2 driving profile, and b) CYC_WVUINTER driving profile

5.4. Bounded load following strategy results

Fig. 14 shows the performance of the BLFS for WLTC_class 2 driving cycle. The requested power from the PEMFC, the battery SOC evolution, the drawn current from the PEMFC, and the stack temperature are shown in Fig. 14a to Fig. 14d respectively. From Fig. 14, it can be observed that all the case studies almost demonstrate similar patterns as the rule-based strategy follows the same policy at all conditions. However, the drawn current from the PEMFC stack seems to be different specifically in the 1D – Aged FC and 1D – FI cases since the aged PEMFC cannot reach the same level of power as the new one and the 1D – FI case receives the false feedback signal.

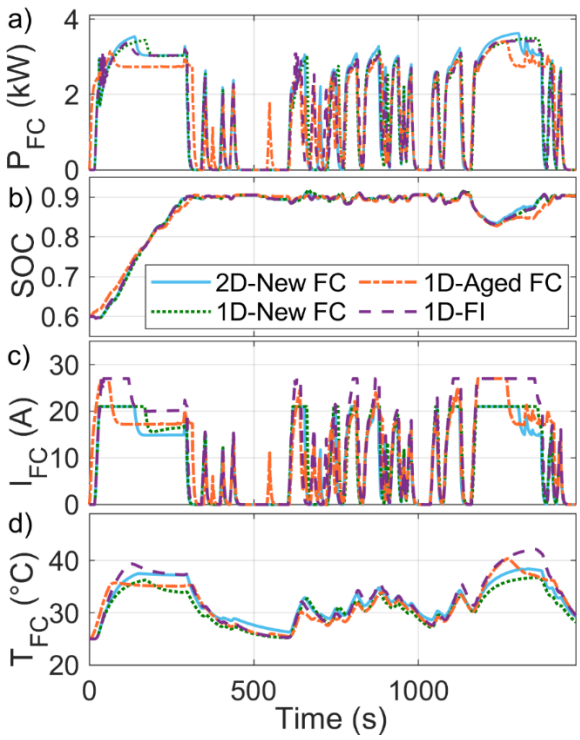

Fig. 14. BLFS results for WLTC_class 2 driving cycle, a) the drawn power from PEMFC stack (scaled-up signal), b) battery SOC, c) the real scale drawn current from the stacks, and d) the real scale stack temperature evolution.

Fig. 15 illustrates the BLFS performance for the CYC_WVUINTER driving cycle. As this driving cycle has more high-speed regimes compared to the WLTC_class 2, the difference between the performance of different cases becomes more evident in this case study. Taking a closer look at Fig. 15c and 15d, it is seen that from 400 s to almost 1100 s, 1D – FI has extracted the highest current from the PEMFC and had the highest stack temperature. The 2D – New FC has almost extracted the lowest current level from the PEMFC for the same time span. To fully comprehend the difference between the performance of the discussed case studies for BLFS, they need to be compared in terms of hydrogen consumption. However, since these cases are based on a real-time strategy, there is no guarantee that they exactly finish in the same final battery SOC. Therefore, to have a fair comparison of hydrogen consumption, each test has been conducted five times starting with different initial SOCs (60%, 65%, 70%, 75%, and 80%). Subsequently, the difference between the initial and final SOC (ΔSOC) versus the hydrogen consumption is plotted. Fig. 16 presents the hydrogen consumption with respect to the battery SOC changes. From this figure, it is observed that the 2D – New FC case has achieved the lowest, and the 1D – FI case has reached the highest hydrogen consumption in both driving cycles regardless of the initial and final battery SOC. Considering ΔSOC = 0.3 in Fig. 16, the following conclusions can be reached:

- Comparison of 1D – New FC and 1D – Aged FC cases indicates that ageing has increased the hydrogen consumption by 3.22% in WLTC_class 2 and 7.02% in CYC_WVUINTER.
- Ignoring the characteristics' update in the PEMFC stack has resulted in a considerable rise in hydrogen consumption. In this regard, comparison of 1D – New FC and 1D – Aged FC with 1D – FI shows that in case of WLTC_class 2, hydrogen consumption has increased by 7.56% and 4.2%, and in case of CYC_WVUINTER, it has increased by 12.14% and 4.78% for the new and aged PEMFC respectively.
- Concerning the influence of temperature dimension integration, comparison of 1D – New FC and 2D – New FC illustrates that the rule-based strategy with two control variables is able to decrease the hydrogen consumption by 3.8% in WLTC_class 2 and 5.37% in CYC_WVUINTER.

The difference between the improvement of hydrogen economy in WLTC_class 2 and CYC_WVUINTER is their different driving speed profiles.

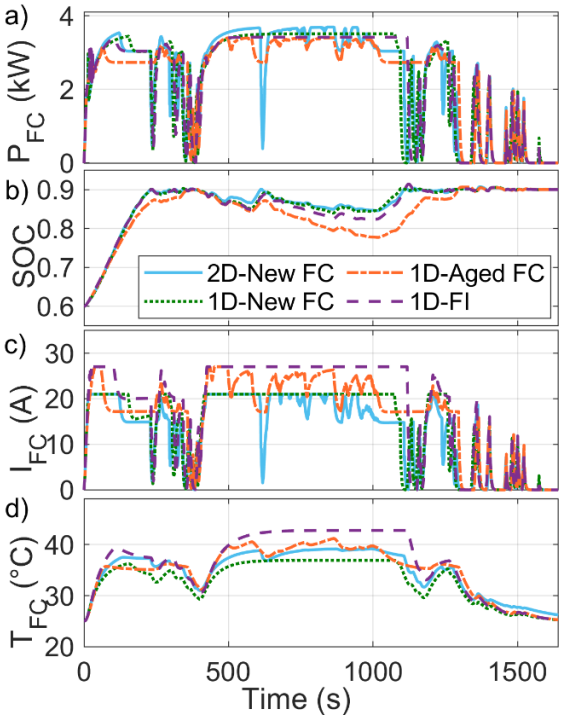

Fig. 15. BLFS results for CYC_WVUINTER driving cycle, a) the drawn power from PEMFC stack (scaled-up signal), b) battery SOC, c) the real scale drawn current from the stacks, and d) the real scale stack temperature evolution.

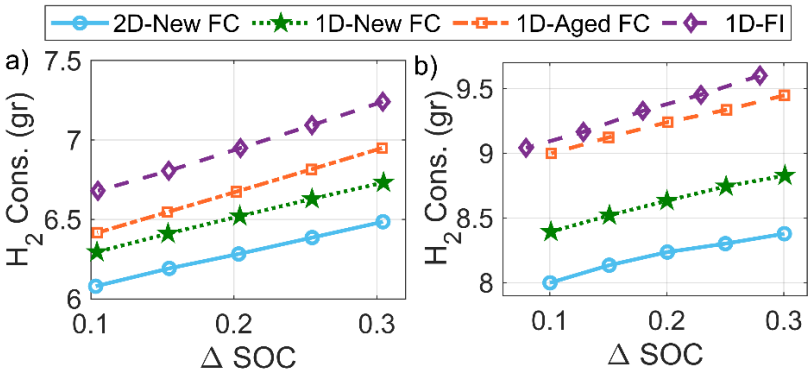

Fig. 16. Hydrogen consumption with respect to the difference between the initial and final battery SOC, a) WLTC_class 2 driving cycle, and b) CYC_WVUINTER driving cycle.

5.5. Synopsis of the obtained results from both EMSs

In order to give a clear understanding of the considered case studies in this paper, a summary of the main conclusions is provided in Table 4. It should be noted that the obtained results from the performed studies in this paper are presented to show the potential of the proposed approach in enhancing the hydrogen economy of FCHEVs. In Table 4, three comparative studies namely 1D – New FC vs. 1D – Aged FC, 1D – Aged FC vs. 1D – FI, and 2D – New FC vs. 1D – New FC are reported. The first one shows the effect of PEMFC ageing on the hydrogen consumption, the second one clarifies the importance of adaptation to health state of the PEMFC during the lifespan of the vehicle, and the last one elucidates the influence of stack temperature dimension consideration in addition to the operating current over hydrogen consumption. It should be noted that the comparisons of 1D – New FC vs. 1D – FI and 2D – New FC vs. 1D – FI have not been considered since they are extreme cases and the anticipated outcomes are obvious in these cases.

The comparison of 1D − New FC vs. 1D − Aged FC shows that hydrogen consumption has increased by different percentages depending on the utilized EMS and driving cycle. One important aspect to point out here is that in case of DP, the percentage of increase in WLTC_class 2 is higher than CYC_WVUINTER. However, in case of BLFS, it is inverse. The difference in the behavior of EMSs is mainly due to the fact that DP determines the best policy depending on the driving cycle while BLFS follows the same rules for both driving cycles. This pattern can also be seen in the second case study (1D − Aged FC vs. 1D − FI) due to the same reason. However, in the third comparative analysis (2D − New FC vs. 1D − FI), it is seen that the percentage of hydrogen consumption decrease in CYC_WVUINTER is higher than WLTC_class 2 for both of DP and BLFS EMSs. This is due to the fact that CYC_WVUINTER driving cycle does not contain a lot of changes which is favorable for allowing the PEMFC stack to reach the. However, WLTC_class 2 driving cycle contains several start-stop cycles and big changes in the speed.

Table 4
The summary of the achieved results by DP and BLFS

Compared case studies	Description	Optimal EMS (DP)		Rule-based EMS (BLFS)	
		WLTC_class 2	CYC_WVUINTER	WLTC_class 2	CYC_WVUINTER
1D − New FC 1D − Aged FC	H_2 consumption increase owing to ageing.	14.7%	11.7%	3.2%	7%
1D − Aged FC 1D − FI	H_2 consumption increase owing to not adapting to the PEMFC health state.	8.7%	7.6%	4.2%	4.7%
2D − New FC 1D − New FC	H_2 consumption decrease due to considering two control variables.	2.9%	4.1%	3.8%	5.3%

6. Conclusion

This paper focuses attention on the influence assessment of a PEMFC stack degradation and thermal management over the fuel economy of a FCHEV. In this respect, a deterministic DP, as an optimal EMS, and BLFS, as a real-time rule-based EMS, are formulated with one and two control variables for a new and an aged PEMFC stack. Similar to the existing EMSs in the literature, the EMS with one control variable only determines the required current from the PEMFC stack, while respecting the limitation of the power sources, and the remainder is supplied by the battery pack. However, the EMS with two control variables determines the required current and stack temperature of the PEMFC stack to supply the power. Considering this temperature dimension in addition to the current is a new step regarding the EMS design which has escaped the attentions in previous studies. The performance of the formulated EMSs is evaluated under two driving profiles of WLTC_class 2 and CYC_WVUINTER. The analysis of various scenarios indicate that the integration of the temperature dimension can enhance the fuel economy up to 4.1% and 5.3% in DP and BLFS respectively. Moreover, the ageing of the PEMFC stack can deteriorate the fuel economy up to 14.7% in DP and 7% in BLFS. The final results also indicate that if the policy of energy management for power distribution between PEMFC and battery is not updated as the PEMFC gets aged, it can increase the hydrogen consumption up to 24.8% in DP and 12.1% in BLFS. Looking forward, future investigations are necessary to validate the kinds of conclusions that can be drawn from the proposed EMS of this work with two control variables by using more complex cost functions including the degradation of PEMFC stack and battery pack. Moreover, as this study shows the potential of an EMS with two control variables in improving the fuel economy of a FCHEV, it is necessary to formulate other common real-time strategies with two control variables to have more realistic perception in real-world cases.

References

[1] K. Handayani, T. Filatova, Y. Krozer, and P. Anugrah, "Seeking for a climate change mitigation and adaptation nexus: Analysis of a long-term power system expansion," *Applied Energy,* vol. 262, p. 114485, 2020/03/15/ 2020.

[2] F. Ülengin, M. Işık, Ş. Ö. Ekici, Ö. Özaydın, Ö. Kabak, and Y. İ. Topçu, "Policy developments for the reduction of climate change impacts by the transportation sector," *Transport Policy,* vol. 61, pp. 36-50, 2018/01/01/ 2018.

[3] W. Zhuang *et al.*, "A survey of powertrain configuration studies on hybrid electric vehicles," *Applied Energy,* vol. 262, p. 114553, 2020/03/15/ 2020.

[4] C. Acar and I. Dincer, "The potential role of hydrogen as a sustainable transportation fuel to combat global warming," *International Journal of Hydrogen Energy,* 2018/11/23/ 2018.

[5] B. Tanç, H. T. Arat, E. Baltacıoğlu, and K. Aydın, "Overview of the next quarter century vision of hydrogen fuel cell electric vehicles," *International Journal of Hydrogen Energy,* vol. 44, no. 20, pp. 10120-10128, 2019/04/19/ 2019.

[6] Z. Li, A. Khajepour, and J. Song, "A comprehensive review of the key technologies for pure electric vehicles," *Energy,* 2019/06/14/ 2019.

[7] N. Sulaiman, M. A. Hannan, A. Mohamed, P. J. Ker, E. H. Majlan, and W. R. Wan Daud, "Optimization of energy management system for fuel-cell hybrid electric vehicles: Issues and recommendations," *Applied Energy,* vol. 228, pp. 2061-2079, 2018/10/15/ 2018.

[8] H. Li, A. Ravey, A. N. Diaye, and A. Djerdir, "A Review of Energy Management Strategy for Fuel Cell Hybrid Electric Vehicle," in *2017 IEEE Vehicle Power and Propulsion Conference (VPPC)*, 2017, pp. 1-6.

[9] Y. Huang *et al.*, "A review of power management strategies and component sizing methods for hybrid vehicles," *Renewable and Sustainable Energy Reviews,* vol. 96, pp. 132-144, 2018/11/01/ 2018.

[10] W. Zhou, L. Yang, Y. Cai, and T. Ying, "Dynamic programming for new energy vehicles based on their work modes Part II: Fuel cell electric vehicles," *Journal of Power Sources,* vol. 407, pp. 92-104, 2018/12/15/ 2018.

[11] W. Zhou, L. Yang, Y. Cai, and T. Ying, "Dynamic programming for New Energy Vehicles based on their work modes part I: Electric Vehicles and Hybrid Electric Vehicles," *Journal of Power Sources,* vol. 406, pp. 151-166, 2018/12/01/ 2018.

[12] R. Zhang and J. Tao, "GA-Based Fuzzy Energy Management System for FC/SC-Powered HEV Considering H2Consumption and Load Variation," *IEEE Transactions on Fuzzy Systems,* vol. 26, no. 4, pp. 1833-1843, 2018.

[13] Y. Liu, J. Li, Z. Chen, D. Qin, and Y. Zhang, "Research on a multi-objective hierarchical prediction energy management strategy for range extended fuel cell vehicles," *Journal of Power Sources,* vol. 429, pp. 55-66, 2019/07/31/ 2019.

[14] S. Xie, X. Hu, Z. Xin, and J. Brighton, "Pontryagin's Minimum Principle based model predictive control of energy management for a plug-in hybrid electric bus," *Applied Energy,* vol. 236, pp. 893-905, 2019/02/15/ 2019.

[15] H. Li, A. Ravey, A. N'Diaye, and A. Djerdir, "A novel equivalent consumption minimization strategy for hybrid electric vehicle powered by fuel cell, battery and supercapacitor," *Journal of Power Sources,* vol. 395, pp. 262-270, 2018/08/15/ 2018.

[16] E. Kamal and L. Adouane, "Intelligent Energy Management Strategy Based on Artificial Neural Fuzzy for Hybrid Vehicle," *IEEE Transactions on Intelligent Vehicles,* vol. 3, no. 1, pp. 112-125, 2018.

[17] R. Zhang, J. Tao, and H. Zhou, "Fuzzy Optimal Energy Management for Fuel Cell and Supercapacitor Systems Using Neural Network Based Driving Pattern Recognition," *IEEE Transactions on Fuzzy Systems,* vol. 27, no. 1, pp. 45-57, 2019.

[18] Z. Sun, Y. Wang, Z. Chen, and X. Li, "Min-max game based energy management strategy for fuel cell/supercapacitor hybrid electric vehicles," *Applied Energy,* vol. 267, p. 115086, 2020/06/01/ 2020.

[19] H. Peng, J. Li, L. Löwenstein, and K. Hameyer, "A scalable, causal, adaptive energy management strategy based on optimal control theory for a fuel cell hybrid railway vehicle," *Applied Energy,* vol. 267, p. 114987, 2020/06/01/ 2020.

[20] N. Bizon, "Real-time optimization strategies of Fuel Cell Hybrid Power Systems based on Load-following control: A new strategy, and a comparative study of topologies and fuel economy obtained," *Applied Energy,* vol. 241, pp. 444-460, 2019/05/01/ 2019.

[21] K. Ettihir, L. Boulon, and K. Agbossou, "Energy management strategy for a fuel cell hybrid vehicle based on maximum efficiency and maximum power identification," *IET Electrical Systems in Transportation,* vol. 6, no. 4, pp. 261-268, 2016.

[22] M. Carignano, V. Roda, R. Costa-Castelló, L. Valiño, A. Lozano, and F. Barreras, "Assessment of Energy Management in a Fuel Cell/Battery Hybrid Vehicle," *IEEE Access,* vol. 7, pp. 16110-16122, 2019.

[23] H. Zhang, X. Li, X. Liu, and J. Yan, "Enhancing fuel cell durability for fuel cell plug-in hybrid electric vehicles through strategic power management," *Applied Energy,* vol. 241, pp. 483-490, 2019/05/01/ 2019.

[24] Y. Wang, Z. Sun, and Z. Chen, "Energy management strategy for battery/supercapacitor/fuel cell hybrid source vehicles based on finite state machine," *Applied Energy,* vol. 254, p. 113707, 2019/11/15/ 2019.

[25] Y. Yan, Q. Li, W. Chen, B. Su, J. Liu, and L. Ma, "Optimal Energy Management and Control in Multimode Equivalent Energy Consumption of Fuel Cell/Supercapacitor of Hybrid Electric Tram," *IEEE Transactions on Industrial Electronics,* vol. 66, no. 8, pp. 6065-6076, 2019.

[26] J. Chen, C. Xu, C. Wu, and W. Xu, "Adaptive Fuzzy Logic Control of Fuel-Cell-Battery Hybrid Systems for Electric Vehicles," *IEEE Transactions on Industrial Informatics,* vol. 14, no. 1, pp. 292-300, 2018.

[27] M. Kandidayeni, A. O. M. Fernandez, A. Khalatbarisoltani, L. Boulon, S. Kelouwani, and H. Chaoui, "An Online Energy Management Strategy for a Fuel Cell/Battery Vehicle Considering the Driving Pattern and Performance Drift Impacts," *IEEE Transactions on Vehicular Technology,* pp. 1-1, 2019.

[28] K. Chen, S. Laghrouche, and A. Djerdir, "Degradation model of proton exchange membrane fuel cell based on a novel hybrid method," *Applied Energy,* vol. 252, p. 113439, 2019/10/15/ 2019.

[29] X. Hu, C. Zou, X. Tang, T. Liu, and L. Hu, "Cost-optimal energy management of hybrid electric vehicles using fuel cell/battery health-aware predictive control," *IEEE Transactions on Power Electronics,* pp. 1-1, 2019.

[30] Y. Wang, S. J. Moura, S. G. Advani, and A. K. Prasad, "Optimization of powerplant component size on board a fuel cell/battery hybrid bus for fuel economy and system durability," *International Journal of Hydrogen Energy,* vol. 44, no. 33, pp. 18283-18292, 2019/07/05/ 2019.

[31] Y. Wang, S. J. Moura, S. G. Advani, and A. K. Prasad, "Power management system for a fuel cell/battery hybrid vehicle incorporating fuel cell and battery degradation," *International Journal of Hydrogen Energy,* vol. 44, no. 16, pp. 8479-8492, 2019/03/29/ 2019.

[32] H. Li, A. Ravey, A. N'Diaye, and A. Djerdir, "Online adaptive equivalent consumption minimization strategy for fuel cell hybrid electric vehicle considering power sources

degradation," *Energy Conversion and Management,* vol. 192, pp. 133-149, 2019/07/15/ 2019.

[33] M. Yue, S. Jemei, R. Gouriveau, and N. Zerhouni, "Review on health-conscious energy management strategies for fuel cell hybrid electric vehicles: Degradation models and strategies," *International Journal of Hydrogen Energy,* vol. 44, no. 13, pp. 6844-6861, 2019/03/08/ 2019.

[34] M. Ehsani, Y. Gao, S. Longo, and K. M. Ebrahimi, "Modern electric, hybrid electric, and fuel cell vehicles : fundamentals, theory, and design," (in English), 2018.

[35] C. Mi, M. A. Masrur, and D. W. Gao, *Hybrid Electric Vehicles: Principles and Applications with Practical Perspectives*. Wiley, 2011.

[36] Y. Zhou, A. Ravey, and M.-C. Péra, "Multi-mode predictive energy management for fuel cell hybrid electric vehicles using Markov driving pattern recognizer," *Applied Energy,* vol. 258, p. 114057, 2020/01/15/ 2020.

[37] R. F. Mann, J. C. Amphlett, M. A. I. Hooper, H. M. Jensen, B. A. Peppley, and P. R. Roberge, "Development and application of a generalised steady-state electrochemical model for a PEM fuel cell," *Journal of Power Sources,* vol. 86, no. 1, pp. 173-180, 2000/03/01/ 2000.

[38] M. Kandidayeni, A. Macias, A. Khalatbarisoltani, L. Boulon, and S. Kelouwani, "Benchmark of proton exchange membrane fuel cell parameters extraction with metaheuristic optimization algorithms," *Energy,* vol. 183, pp. 912-925, 2019/09/15/ 2019.

[39] K. Ou, W.-W. Yuan, M. Choi, S. Yang, and Y.-B. Kim, "Performance increase for an open-cathode PEM fuel cell with humidity and temperature control," *International Journal of Hydrogen Energy,* vol. 42, no. 50, pp. 29852-29862, 2017/12/14/ 2017.

[40] Y.-X. Wang, F.-F. Qin, K. Ou, and Y.-B. Kim, "Temperature Control for a Polymer Electrolyte Membrane Fuel Cell by Using Fuzzy Rule," *IEEE Transactions on Energy Conversion,* vol. 31, no. 2, pp. 667-675, 2016.

[41] J. Larminie, "Efficiency and Open Circuit Voltage," in *Fuel Cell Systems Explained*, A. Dicks and Knovel, Eds.: J. Wiley, 2003, pp. 25-43.

[42] L. Guzzella and A. Sciarretta, *Vehicle Propulsion Systems: Introduction to Modeling and Optimization*. Springer, 2005.

[43] M. Kandidayeni, A. Macias, L. Boulon, and S. Kelouwani, "Efficiency Enhancement of an Open Cathode Fuel Cell through a Systemic Management," *IEEE Transactions on Vehicular Technology,* pp. 1-1, 2019.

[44] V. H. Johnson, "Battery performance models in ADVISOR," *Journal of Power Sources,* vol. 110, no. 2, pp. 321-329, 2002/08/22/ 2002.

[45] V. H. Johnson, A. A. Pesaran, and T. Sack, *Temperature-Dependent Battery Models for High-Power Lithium-Ion Batteries* (Conference: 17th Annual Electric Vehicle Symposium, Montreal, Quebec (CA), 10/15/2000--10/18/2000; Other Information: PBD: 10 Jan 2001). ; National Renewable Energy Lab., Golden, CO (US), 2001, p. Medium: ED; Size: vp.

[46] O. Sundstrom and L. Guzzella, "A generic dynamic programming Matlab function," in *2009 IEEE Control Applications, (CCA) & Intelligent Control, (ISIC)*, 2009, pp. 1625-1630.

[47] K. Ettihir, L. Boulon, and K. Agbossou, "Optimization-based energy management strategy for a fuel cell/battery hybrid power system," *Applied Energy,* vol. 163, pp. 142-153, 2016/02/01/ 2016.